ELSEVIER

Nuclear Physics A 629 (1998) 635-655

NUCLEAR PHYSICS A

Projectile-fragment yields as a probe for the collective enhancement in the nuclear level density ★

A.R. Junghans [a], M. de Jong [a], H.-G. Clerc [a], A.V. Ignatyuk [b], G.A. Kudyaev [b], K.-H. Schmidt [c]

[a] *Inst. für Kernphysik, Technische Universität Darmstadt, Schloßgartenstraße 9, 64289 Darmstadt, Germany*
[b] *Inst. of Physics and Power Engineering, Bondarenko Square, 249020 Obninsk, Kaluga Region, Russia*
[c] *Gesellschaft für Schwerionenforschung, Planckstraße 1, 64291 Darmstadt, Germany*

Received 19 September 1997; revised 1 December 1997; accepted 2 December 1997

Abstract

Production cross sections of several hundred nuclei produced in the fragmentation of uranium and lead projectiles are analysed with the abrasion–ablation model taking into account fission in the deexcitation chain. The survival probability against fission of excited compound nuclei is a sensitive probe for shell and collective effects in the nuclear level density. The expected stabilization against fission for neutron-deficient actinides near the magic number $N = 126$ due to large ground-state shell effects is not found in the experimental data. With the inclusion of collective enhancement in the level density the experimental data can be described well. The damping of the collective enhancement with excitation energy has to be treated as essentially independent of nuclear deformation, a new finding which contradicts the current theoretical picture. A schematic description of the vibrational enhancement in spherical nuclei is deduced from the data. The lack of shell stabilization against fission observed for the 126-neutron shell is expected to have consequences for the production cross sections of spherical superheavy elements around $N = 184$. © 1998 Elsevier Science B.V.

PACS: 25.70.Mn; 25.85.-w; 21.10.Ma; 21.10.Re
Keywords: Projectile fragmentation; ^{238}U (950 A MeV)+Cu; Nuclear level density; Collective enhancement; Production of superheavy elements

★ This work forms part of the dissertation of A.R. Junghans.

PII S0375-9474(98)00658-1

1. Introduction

One of the fundamental questions of nuclear physics that did not yet find an answer, is up to which excitation energies collective nuclear excitations may persist. Several theoretical estimations have been proposed for the loss of collectivity of nuclear excitations as a function of nuclear temperature (e.g. Refs. [1,2]), but no experimental verification has been performed up to now. With the analysis carried out in the present work we try to find an answer to this question.

Direct information on collective excitations is usually obtained by analysing the transitions between excited states. In nuclear spectroscopy, spin, parity and the excitation-energy pattern of excited levels as well as transition rates give an indication on the collectivity of the excitation. However, individual transitions can be observed at energies close to the yrast line, only. At higher excitation energies, where nuclear levels strongly overlap, the collectivity of nuclear excitations may still be studied by its influence on the statistical properties of nuclei. Such an approach is widely used in molecular physics, where collective rotational bands and phonon vibrational excitations are clearly identified. They couple to electronic excitations and increase the statistical sum. Basically the same classes of excitations are observed in nuclei: collective rotations and vibrations with many nucleons involved couple to single-particle excitations of individual nucleons. Collective excitations of nuclei have successfully been described in the unified model, introduced by Bohr and Mottelson [3,4]. Any contribution of collective excitations is expected to manifest itself as an enhancement of the nuclear level density. Enhancement factors in the order of 10, for vibrational excitations, and in the order of 100, for rotational bands, are predicted in the adiabatic limit [1]. Therefore, an indication for the collectivity of nuclear excitations may be deduced by comparing the measured density of nuclear levels to the calculated density of single-particle excitations. A realistic description of the single-particle excitations and a reliable experimental determination of the nuclear level density are the prerequisites for this approach.

The most reliable information on *absolute* nuclear level densities originates from counting low-lying levels and from neutron resonances. These data clearly reveal the strong influence of nuclear shell effects: the density of resonances is very much reduced in magic nuclei [5–7]. A quantitative understanding of these fluctuations has been achieved in the independent-particle model [8–12]. As an analytic approximation to microscopic calculations, an exponential washing out of shell effects in the level density with increasing excitation energy has been deduced [11,13]. A quantitative analysis of the neutron-resonance data also revealed the contribution of collective excitations at excitation energies around 7 MeV [14].

The ratio of statistical decay rates of different deexcitation channels from excited nuclei represents an important information on *relative* level densities. These data are also available at higher excitation energies. The competition between different evaporated particles (e.g. neutrons, protons, α particles) relates the level densities of similar nuclei which often have similar properties like deformations or shell effects. Data on fission probabilities are particularly important for the understanding of structural effects in the

nuclear level density, because they relate the level densities of neighbouring nuclei in very different configurations: the level density of the fissioning nucleus above the fission barrier and that of the daughter nucleus after neutron evaporation in its ground-state shape. Measured fission probabilities have served to deduce collective contributions to the level density at the saddle-point deformation at energies of a few MeV above the fission barrier [15] and to investigate the influence of ground-state shell effects in transuranium nuclei [16]. However, fission probabilities also represent a unique source of information on the collective excitations at the ground-state deformation. In the ground-state configuration, both the shell effect and the symmetry class vary strongly as a function of neutron or proton number, whereas the shell effects at the saddle point are expected to be small and the shape is always strongly deformed. Thus, by analysing fission probabilities of different nuclei, the level density in the strongly deformed saddle point serves as a reference for structural and collective effects in nuclei with spherical or deformed shapes in the ground state.

Many results on fission probabilities have been accumulated for nuclei around ^{208}Pb [17–20]. However, due to the high fission barriers of these nuclei, they could be measured only at excitation energies larger than 20 MeV. It has been shown that these data can well be described without considering any collective excitations when a "backshift" in the level density is introduced which corresponds to the ground-state shell effect in the nuclear binding energy [21,20]. Since this procedure eliminates any influence of shell effects on the model calculation, it is equivalent to a complete washing out of shell effects in the level density. Rather opposite conclusions were drawn in other studies, where shell effects and collective excitations were included [14,19,16]. It seems difficult to extract more conclusive information from these data, due to the high fission barriers involved.

Proton-rich nuclei near the 126-neutron shell are expected to have appreciably lower fission barriers and thus offer a unique possibility to study the fission probability of magic nuclei at low excitation energies. But also the measured cross sections of evaporation residues around ^{216}Th, produced in heavy-ion fusion reactions [22,23] did not show any noticeable enhancement due to the shell stabilization around $N = 126$, although a strong shell effect of around 5 MeV is clearly seen in the ground-state masses which can be estimated on the basis of measured Q values for α decay. This result is in sharp contrast to expectations based on the intrinsic level densities calculated in the independent-particle model. The lack of stabilization against fission around $N = 126$ found in the data has been explained by the influence of collective excitations, either in terms of a reduced collective contribution to the level density in spherical nuclei [24] or by the idea of a temperature-induced deformation [25].

The present work resumes this problem by using data from a different nuclear reaction, namely the fragmentation of relativistic heavy ions. The measured production cross sections of ^{238}U projectile fragments in the vicinity of the 126-neutron shell [26] are compared to model calculations in order to deduce the level densities of magic and non-magic nuclei. The level density is tested down to energies around the fission barrier.

If compared to fusion reactions, the projectile fragmentation has two important ad-

vantages. First, long chains of nuclei crossing the 126-neutron shell are simultaneously produced. Secondly, the induced angular momentum in peripheral reactions of relativistic heavy ions is low, of the order of 10 to 20 $\hbar$, as has been shown by statistical calculations based on the shell model [27]. In contrast, the analysis of fusion-reaction residues was complicated by entrance-channel effects and by high angular momenta which both are specific for each target-projectile combination [28]. Therefore, it should be possible to study the expected enhancement in the production of shell-stabilized nuclei with much higher sensitivity from the new projectile-fragmentation data than from the heavy-ion fusion reactions used previously. The excitation energies induced in the fragmentation reaction range from low values up to several hundred MeV. Nevertheless, the data allow to deduce structural effects in the level density at low excitation energies very well, because the resulting cross sections depend on the product of the survival probabilities in the different deexcitation steps. While no structural effects are expected at higher excitation energies, nuclear structure has an important influence on the last steps of the deexcitation process, and the corresponding survival probabilities fully enter into the production cross sections. Thus, the data clearly reflect the influence of nuclear structure at low excitation energies.

2. Method

Cross sections for the production of several hundred different projectile fragments in the reactions ^{238}U(950 A MeV)+Cu [29,26] and ^{208}Pb(1000 A MeV)+Cu [29,30] have been measured at the fragment separator FRS of GSI, Darmstadt. Part of these cross sections is analysed to find structural effects in the level density of these nuclei.

The analysis is based on a modern version of the geometrical abrasion–ablation model [31] with the inclusion of fission. Peripheral collisions of relativistic heavy ions are treated as a two-step process in this model. In the first abrasion step the nucleons in the overlap zone of projectile and target are violently and suddenly removed, and the non-overlapping part, the prefragment, will form an excited compound nucleus which deexcites in the second reaction step by particle evaporation or fission.

Depending on the impact parameter of the collision, a distribution of intermediate prefragments is formed by abrasion. The mass loss is determined by integration of the overlap volume, and the excitation-energy distribution is directly related to the mass loss. By comparison with experimental production cross sections from gold fragmentation, the mean excitation energy per abraded nucleon was found to be 27 MeV [32]. From measurements of the Aladin Group at GSI Darmstadt, comparable values of 20–24 MeV per abraded nucleon for peripheral collisions have been derived [33].

In order to draw conclusions concerning the deexcitation phase it is necessary to have a thorough understanding of the abrasion process which produces the highly excited compound nuclei studied in this work. This has been the object of several previous studies [31,34,32,27].

Here we only want to demonstrate that we have gained a good description of the

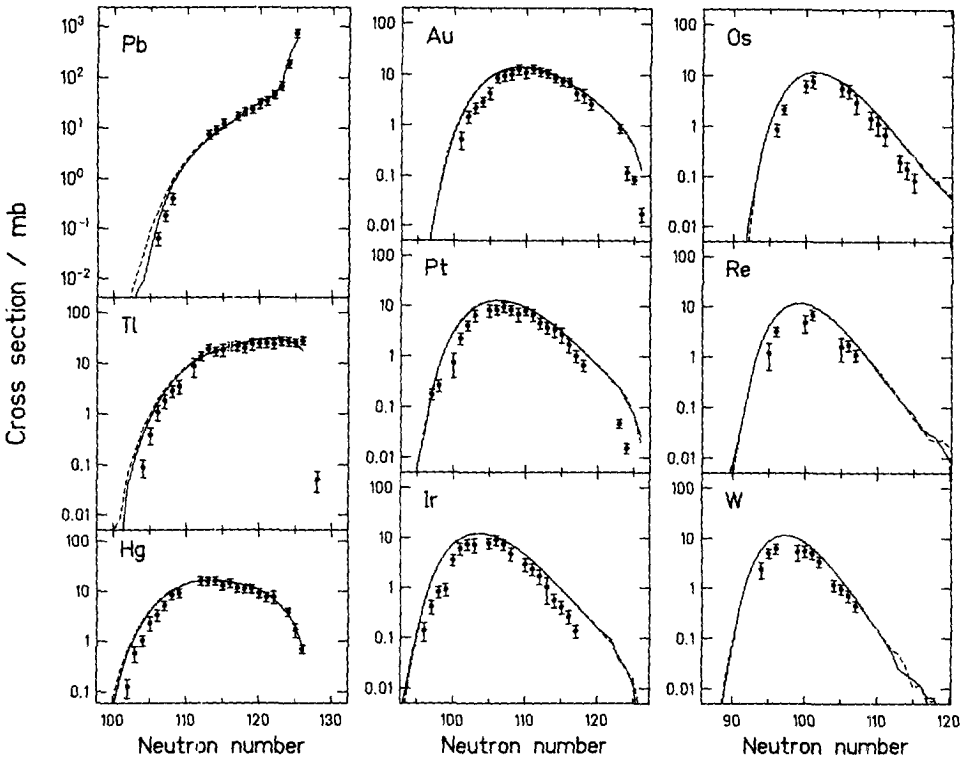

Fig. 1. Measured cross sections of projectile fragments produced by a 1 A GeV ^{208}Pb beam in a copper target. The data (data points) are compared to a model calculation including fission (dashed lines). For comparison, another calculation has been performed without the inclusion of the fission competition (full lines).

fragmentation process of heavy nuclei by the abrasion–ablation model, as is shown in Fig. 1 for lead fragmentation. It may be seen that the calculations with and without the fission channel give an equally good description. This means on the one hand that fission is not an important reaction channel in the fragmentation of lead projectiles, and on the other hand that the fragmentation process of heavy projectiles is well understood. Therefore, we have a reliable basis for our current investigation of structural effects in the level density of uranium projectile fragments.

The details how the fission channel is treated in the abrasion–ablation model including the influence of dissipative effects on fission at high excitation energies are discussed in Ref. [35]. Here we want to recapitulate the most important parameters in the calculation of the fission probability.

Based on the single-particle schemes of the Woods–Saxon potential the asymptotic level-density parameter $\tilde{a}$ is calculated according to Ignatyuk et al. [36]. For the saddle-point deformation, the asymptotic level-density parameter $\tilde{a}_f$ is approximately 4–5 (2–3) percent larger than $\tilde{a}_n$ at the ground-state deformation for nuclei with mass number $A \approx 200$ (230).

The fission barriers are calculated in a macroscopic-microscopic approach. The macro-

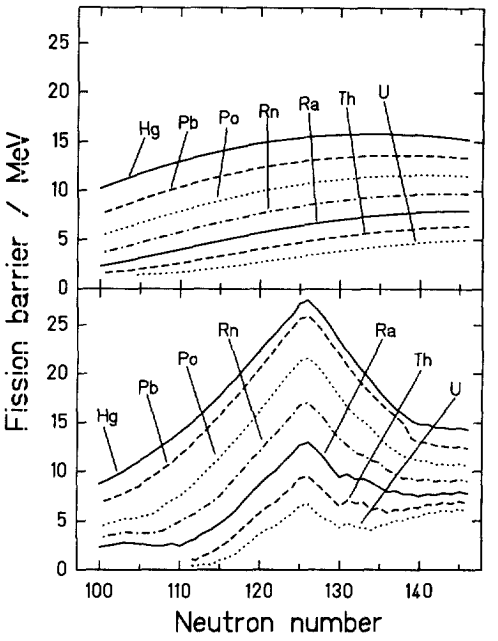

Fig. 2. Fission barriers of nuclei in the region of interest for the present investigation. Upper part: The macroscopic part [37] of the fission barrier at zero angular momentum. Lower part: The curves include the contribution of the ground-state shell effect [38].

scopic part is calculated from the rotating finite-range liquid-drop model [37] and is displayed in the upper part of Fig. 2. The ground-state shell effects are calculated as the difference between the calculated ground-state atomic mass excess and the corresponding macroscopic value from the finite-range liquid-drop model [38]. By adding the ground-state shell effect to the macroscopic part of the fission barrier, the total fission barriers as shown in the lower part of Fig. 2 are obtained. Any shell effects at the saddle point are assumed to be small and negligible. Since projectile fragments are produced with low angular momenta, about 10 to 20 $\hbar$ [27], the influence of angular momentum on fission in fragmentation reactions is negligible.

The fragmentation of uranium projectiles has already been investigated before, and the cross sections for the production of uranium and protactinium isotopes were found to be reduced by several orders of magnitude due to the influence of fission [29]. In Fig. 3, one can see that the calculation without fission predicts far too high production cross sections for uranium projectile fragments from uranium down to bismuth.

In the following we will investigate the influence of shell effects and collective degrees of freedom on the survival probability of uranium projectile fragments against fission. We will introduce the effects to be discussed separately one after the other in order to demonstrate the magnitude of the effects on the experimental data. First, we will discuss the intrinsic level density including shell corrections, then we will introduce collective contributions to the level density, namely the rotational enhancement for deformed nuclei, and, in a further step, the vibrational enhancement for spherical shapes.

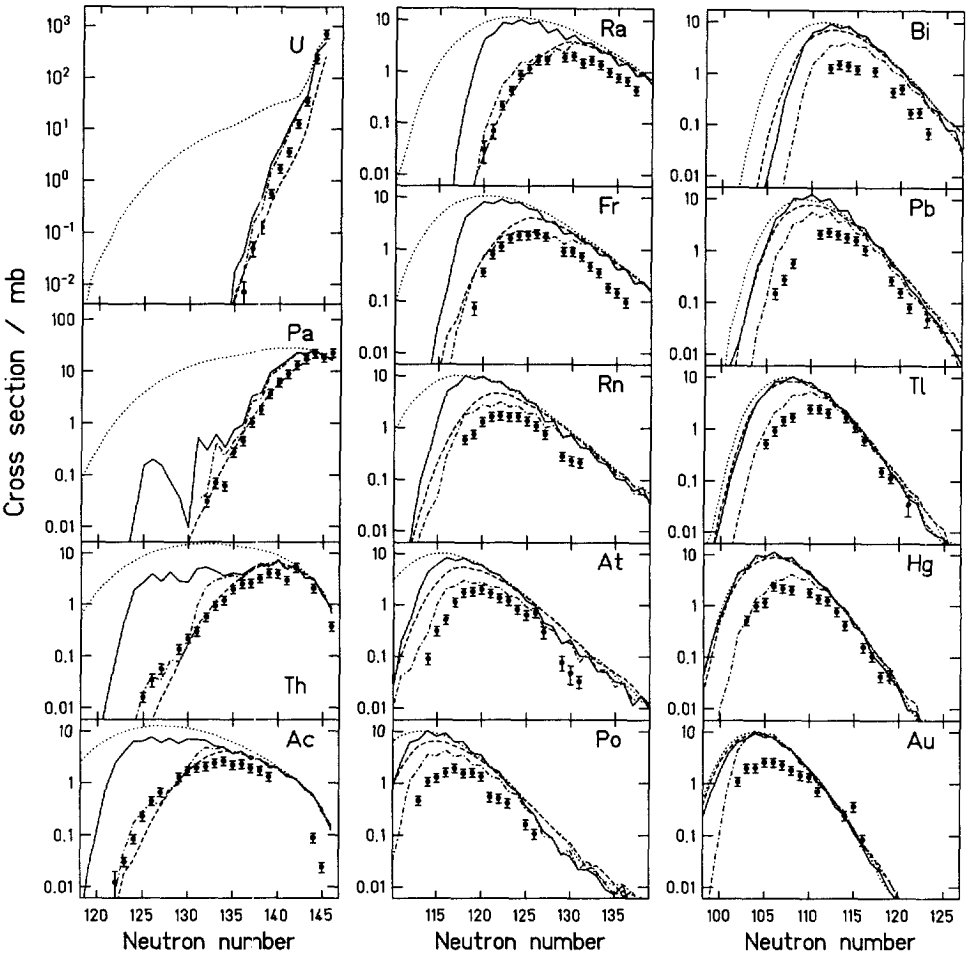

Fig. 3. Measured cross sections of projectile fragments produced by a 950 AMeV ^{238}U beam in a copper target (data points). The data are compared to different model calculations, disregarding any shell effects in binding energies and level densities (dashed lines), using intrinsic level densities including shell effects (full lines), and including collective excitations (dash-dotted lines). For comparison, another calculation has been performed without the inclusion of the fission competition (dotted lines).

3. Intrinsic level density and shell corrections

At first we will compare the data with a calculation based on a pure Fermi-gas level density (see Appendix A for details). Microscopic corrections for shell and pairing effects in the masses, in the fission barriers, in the particle separation energies, as well as in the level densities are not included. The dashed lines in Fig. 3 show that this calculation describes the data very well, especially for nuclei around the 126-neutron shell where one would expect a stabilization against fission in the deexcitation process due to large ground-state shell effects of about 5 MeV. As a matter of fact, the data do not show any enhancement in the production cross section around the neutron shell.

The next step is to add the shell and pairing corrections. The combination of a Fermi-gas level density with microscopic corrections for shell and pairing in an analytical approximation is a widely used approach to predict the level density without numerically solving a microscopic model for definite single-particle levels [21]. Ignatyuk et al. [11] and Schmidt et al. [13] have demonstrated the validity of this method and compared the analytical approximation for the shell correction with microscopical calculations for nuclei around $N = 126$.

The full lines in Fig. 3 show the expected strong enhancement in the predicted production cross sections of more than one order of magnitude for nuclei around $N = 126$, e.g. thorium and actinium isotopes, if shell and pairing effects are included. However, this calculation is in sharp contradiction to the experiment. Somehow, the magic nuclei seem to loose their stabilization against fission at considerably lower excitation energies than predicted on the basis of the intrinsic level densities. The fission probability for nuclei around $N = 126$ cannot be described correctly in this approach.

4. Collective enhancement

A deeper understanding of this result may be obtained by taking the collective properties of nuclei into consideration. Bjørnholm, Bohr, and Mottelson have discussed how the symmetry class of the nuclear shape defines the collective degrees of freedom and to what extent collective excitations contribute to the nuclear level density [1]. They found that the total level density including collective and intrinsic excitations $\rho(E)$ can be expressed by the level density of intrinsic excitations $\rho_{\mathrm{intr}}(E)$ multiplied by a collective enhancement factor $K_{\mathrm{coll}}(E)$:

$$\rho(E) = K_{\mathrm{coll}}(E)\rho_{\mathrm{intr}}(E) .$$

In deformed nuclei the most important contribution to the collective enhancement of the level density originates from rotational bands, in spherical nuclei the collective enhancement is caused by vibrational excitations. In a complete survey, the problem would be even more complex, because the collective enhancement of the level density has to be estimated not only for spherical and well deformed but also for transitional nuclei, where the collective character (rotational or vibrational) is not well defined. In addition, the mean deformation may vary with excitation energy.

4.1. Rotational enhancement

For ground-state deformed nuclei in the actinide region, the largest contribution to the collective enhancement is due to rotational bands built up on intrinsic states. This rotational enhancement can reach two orders of magnitude, see Fig. 4.

With increasing excitation energy, the rotational enhancement is expected to be damped, because a separation between intrinsic and collective rotational motion can only be made at temperatures which are low enough to ensure a well defined deforma-

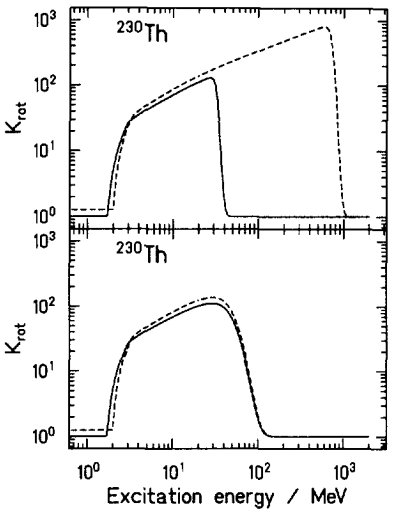

Fig. 4. The rotational enhancement factor $K_{\rm rot}(E)$ as a function of excitation energy for the nucleus ^{230}Th in the ground-state deformation (full lines) and in the saddle-point deformation (dashed lines). The upper part is calculated with parameters of Ref. [2], which are strongly deformation dependent, while the lower part is calculated with parameters which are independent of deformation as proposed in this work.

tion of the nucleus. This was already pointed out in Ref. [1] and more elaborately in Ref. [2].

For nuclei with a quadrupole deformation $|\beta_2| > 0.15$ we calculate the rotational enhancement factor in terms of the spin-cutoff parameter $\sigma_\perp$:

$$K_{\rm rot}(E) = \begin{cases} (\sigma_\perp^2 - 1) f(E) + 1 & \text{for } \sigma_\perp^2 > 1\,, \\ 1 & \text{for } \sigma_\perp^2 \leqslant 1\,, \end{cases}$$
$$\sigma_\perp^2 = \frac{\mathcal{J}_\perp T}{\hbar^2}\,, \qquad (1)$$
$$f(E) = \left(1 + \exp\left(\frac{E - E_{\rm cr}}{d_{\rm cr}}\right)\right)^{-1}\,.$$

Here $\mathcal{J}_\perp = \frac{2}{5} m_0 A R^2 (1 + \beta_2/3)$ is the rigid-body moment of inertia perpendicular to the symmetry axis, with A the nuclear mass number, $R = 1.2$ fm $A^{1/3}$ the nuclear radius, and m_0 the mass unit. T denotes the nuclear temperature. The ground-state quadrupole deformation β_2 is taken from the finite-range liquid-drop model including microscopic corrections [38], while the saddle-point deformation is taken from the liquid-drop model as given in Ref. [39].

Eq. (1) is valid for nuclei which are both axially- and mirror-symmetric. For other symmetry classes (e.g. triaxial shapes), different rotational enhancement factors should be applied [1], but as the actual ground-state shape of most of the neutron-deficient nuclei discussed here is not known, we use the expression for axially- and mirror-symmetric shapes as an approximation. The same symmetry class is used to describe the saddle-point deformations.

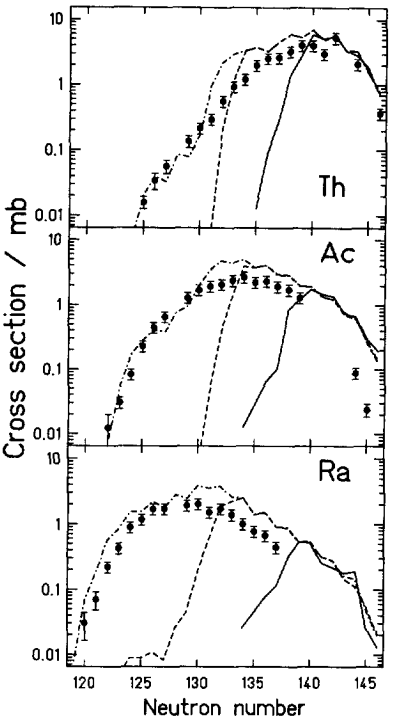

Fig. 5. Production cross sections of thorium, actinium, and radium fragments from a 950 A MeV ^{238}U beam in a copper target are shown as data points. The full lines show a calculation including rotational enhancement for ground-state deformed nuclei with the damping of $K_{\rm rot}(E)$ according to Hansen and Jensen [2]. The dashed lines are calculated with rotational enhancement but with damping independent of deformation (this work), and the dash-dotted lines include in addition vibrational enhancement for nuclei with a spherical ground state.

The damping of the collective modes with increasing excitation energy is described by a Fermi function $f(E)$ which requires two parameters, a critical energy $E_{\rm cr}$ at which $f(E_{\rm cr}) = 0.5$, and the width parameter $d_{\rm cr}$. Based on a SU(3) shell model with a two-body quadrupole-quadrupole interaction, Hansen and Jensen found that these parameters substantially depend on the magnitude of the deformation [2]:

$$E_{\rm cr} = 120\ \text{MeV}\ \beta_2^2 A^{1/3}, \qquad d_{\rm cr} = 1400\ \text{MeV}\ \beta_2^2/A^{2/3}.$$

The excitation-energy dependence of the rotational enhancement factor $K_{\rm rot}(E)$ calculated for ^{230}Th with these parameters is shown in the upper part of Fig. 4 for the ground-state deformation ($\beta_2 = 0.198$) and for the saddle-point deformation ($\beta_2 \approx 0.98$). The rotational enhancement at the saddle point pertains to significantly higher excitation energy than the rotational enhancement at the ground-state deformation. In Fig. 5 one can see that an abrasion–ablation model calculation using this strongly deformation-dependent approach cannot describe our data. Even for ground-state deformed thorium, actinium, and radium isotopes with $N = 135-140$ the predicted yields fall off rapidly, which is a result of the high fission probability due to the rotational enhancement still in effect at the saddle-point deformation at high excitation energy (>40 MeV).

The damping with excitation energy seems to be far too weak at large deformations (e.g. the critical energy amounts to 706 MeV for the saddle-point ($\beta_2 \approx 0.98$) of ^{230}Th), see upper part of Fig. 4. Therefore, we propose to use a damping *independent of deformation* with $E_{cr} = 40$ MeV, $d_{cr} = 10$ MeV, which corresponds to the predicted values for ground-state deformed nuclei ($\beta_2 \approx 0.2-0.3$, $A \approx 230$), also for the saddle-point deformation, see the lower part of Fig. 4. Using these values, we have achieved a good description for the rotational enhancement of the level density in nuclei which are deformed in their ground states with neutron numbers $N \gtrsim 132$, see Fig. 5 (dashed lines). However, from our analysis the damping with excitation energy of the rotational enhancement is found to be essentially *independent of deformation* which is in contrast to the theoretical prediction of Refs. [1,2].

4.2. Vibrational enhancement

Now we have to focus on nuclei with spherical or nearly spherical ground states around the magic 126-neutron shell, for which the calculated cross sections with the inclusion of rotational enhancement fall drastically below the data, see Fig. 5. This discrepancy may be explained by the influence of vibrational excitations. The vibrational enhancement for spherical nuclei is generally smaller than the rotational enhancement for deformed nuclei. The theoretically stringent description of the vibrational enhancement is complicated by the fact that for the nuclei involved here the collective properties are not sufficiently well known, i.e. for the proton-rich actinides around $N = 126$.

Therefore, we have introduced an effective vibrational enhancement factor $K_{vib}(E)$ formulated on the basis of the functional dependence of $K_{rot}(E)$ to describe the collective behaviour of nuclei with a ground-state quadrupole deformation of $|\beta_2| < 0.15$:

$$K_{vib}(E) = 25\beta_{eff}^2 K_{rot}(E)\,. \tag{2}$$

By this formula the damping of the vibrational enhancement with excitation energy is supposed to be the same as the damping of the rotational enhancement, see Eq. (1). In addition $K_{vib}(E)$ is required to be greater or equal than 1. The rotational enhancement factor $K_{rot}(E)$ is multiplied with the square of a dynamical deformation parameter β_{eff} with

$$\beta_{eff} = 0.022 + 0.003\Delta N + 0.005\Delta Z\,,$$

where $\Delta N(\Delta Z)$ are the absolute values of the number of neutrons (protons) above or below the nearest shell closure. In this way the rigid-body moment of inertia $\mathcal{J}_\perp$ used in Eq. (1) is substituted by the irrotational-flow value of a liquid drop ($\mathcal{J}_{irr} = \beta_{eff}^2 \mathcal{J}_\perp$) [10] to simulate the vibrational motion. The factor 25 is chosen to fit the experimental data shown in Figs. 3 and 5. With the addition of the vibrational enhancement to the level density as parametrized by Eq. (2), the experimental production cross sections can be described well, as shown in Figs. 3 and 5 (dashed-dotted lines).

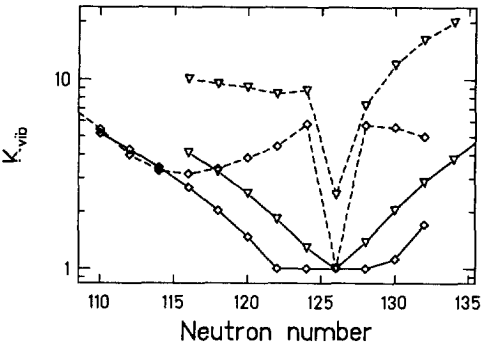

Fig. 6. The vibrational enhancement factor K_{vib}^{ad} (Eq. (3)) as calculated for quadrupole vibrations shown for even lead (diamonds) and polonium (triangles) isotopes connected with dashed lines. The effective vibrational enhancement from Eq. (2) is shown for the same nuclei with full connecting lines.

The collective enhancement for nuclei which are known to be good vibrators can be calculated from the vibrational statistical sum [1]. Regarding quadrupole vibrations one obtains in the adiabatic approximation:

$$K_{vib}^{ad} = \left(1 - \exp\left(\frac{-E_1(2^+)}{T}\right)\right)^{-5}, \tag{3}$$

with the energy of the first excited 2^+ level $E_1(2^+)$ of the nucleus and T, the nuclear temperature. The values of K_{vib}^{ad} are shown in Fig. 6 for the even–even isotopes of lead and polonium. The $E_1(2^+)$ values were taken from the compilation [40] and an excitation energy of 8 MeV corresponding to a temperature T = 0.6–0.7 MeV was chosen.

In Fig. 6 it is shown that the vibrational enhancement calculated with our parametrization for the lead and polonium isotopes is on the average smaller than the theoretical prediction of Eq. (3) and shows a smoother behaviour around the shell. The values of $K_{vib}(E)$ needed to describe our data may be considered as an empirical information on the level density of the spherical actinides around the 126-neutron shell in an excitation-energy range below 40 MeV.

5. Discussion

5.1. Density of excited states in $^{216,222,230}Th$

Densities of excited states as discussed in the preceding sections are shown in Fig. 7 for three characteristic cases: the spherical ^{216}Th at the 126-neutron shell, the transitional ^{222}Th, and the ground-state deformed ^{230}Th. In contrast to the level density, the state density takes the degeneracy of nuclear levels into account, and thus represents the statistical weight of nuclear excitations. The energy scale has a macroscopic reference, i.e. the origin is a fictitious liquid-drop nucleus without any shell structure. The shell effects at the saddle point are assumed to be small and are disregarded completely. As

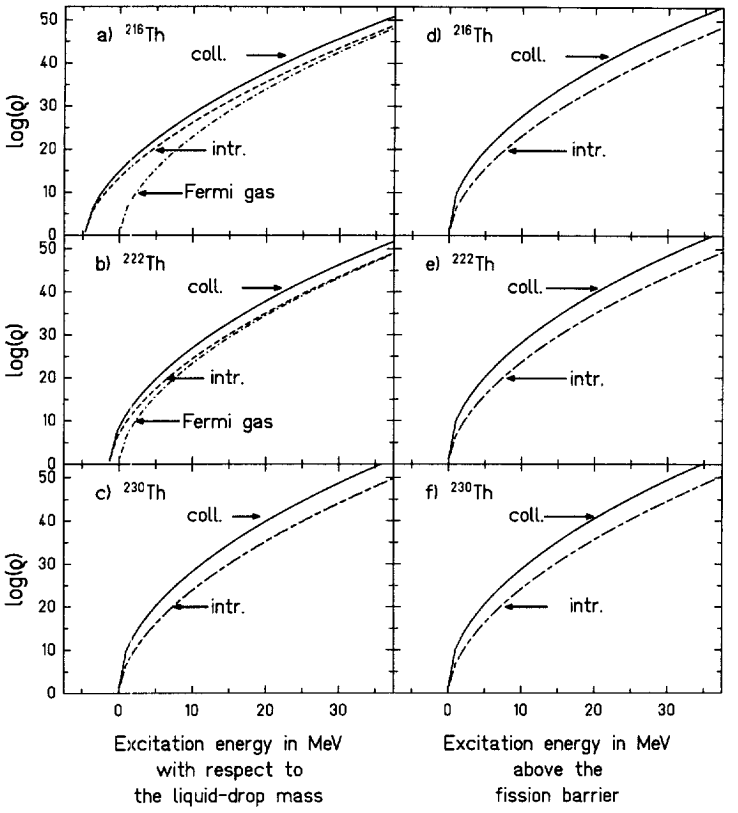

Fig. 7. State density above the ground state (left) and above the saddle point (right) for a nucleus with a spherical, a transitional and a deformed ground state. The state density of the spherical nucleus ^{216}Th (a), of the transitional nucleus ^{222}Th (b), and of the deformed nucleus ^{230}Th (c) as predicted by different approaches: intrinsic state density including the shell correction (dashed lines), full state densities including shell corrections and collective levels (full lines). For comparison, the state density of corresponding fictitious nuclei without any shell effect is shown (Fermi gas). Parts (d), (e) and (f) show the corresponding predictions without and with collective enhancement for the state density at the saddle point, assuming a prolate, rotational symmetric shape. In parts (c), (d), (e), (f) the calculations with and without shell effects (intr. and Fermi gas) can not be distinguished in the figure and coincide on one line.

a consequence, these nuclei have very similar state densities above the saddle point, but remarkable differences in the state densities above the respective ground state.

The state densities calculated with the Fermi-gas expression above the liquid-drop potential are very similar in all cases, just depending slightly on mass and deformation. These curves may serve as a reference for the further discussion. In the cases of vanishing shell effects, these curves coincide with the calculated intrinsic state densities.

The influence of a strong ground-state shell effect on the intrinsic state density is illustrated for ^{216}Th. The ground state is shifted by -5 MeV due to the additional binding. Furthermore, the intrinsic state density including shell effects is enhanced over the whole energy range. This enhancement is washed out exponentially with increasing excitation energy. Since shell effects at the fission barrier are neglected, the state density

above the saddle is not modified by shell effects. Thus, the inclusion of the shell stabilization in the intrinsic state density leads to a considerable enhancement of the statistical neutron decay rate and, consequently, to a stabilization against fission. This effect is smaller in ^{222}Th due to the smaller shell correction, and it vanishes in ^{230}Th.

When collective excitations are included, the state densities of all nuclei in both configurations are enhanced. However, this enhancement strongly depends on the symmetry class of the configuration. While the collective enhancement is essentially the same at the saddle-point deformation for all nuclei, it differs very much in the ground-state deformation for the three representative nuclei. For the well deformed nucleus ^{230}Th, the collective enhancement factors for both configurations, above the saddle point and above the ground state, are almost equal. They both represent the effect of rotational excitations. Thus, the inclusion of collective excitations does not have any noticeable influence on the fission probability of well deformed nuclei. The situation is different for the magic ^{216}Th where the collective excitations in the spherical ground-state deformation have a vibrational character. The vibrational enhancement factor to be applied in spherical configurations is much smaller than the rotational enhancement factor applied in deformed configurations. Thus, the inclusion of collective excitations in spherical nuclei enhances the state density at the saddle-point deformation much more than above the ground state and consequently leads to an increased fission competition in the deexcitation chain. This increase approximately compensates for the shell stabilization of the intrinsic state density. The transitional nucleus ^{222}Th represents an intermediate case. A comparison with the respective Fermi-gas prediction reveals that the state densities including shell effects and collective excitations finally are very similar for all three thorium isotopes, except at very low excitation energies. As a result, the shell stabilization against fission expected on the basis of the intrinsic level density vanishes, if collective excitations are included.

The state densities including shell effects and collective excitations are all higher by about the same factor if compared to the state densities calculated with the Fermi-gas expression above the liquid-drop potential. This is the reason why the liquid-drop calculation and the full calculation including shell effects and collective excitations predict about the same cross sections which agree with the experimental values.

5.2. Consequences for the production of superheavy elements

The observation that large ground-state shell effects of the spherical 126-neutron shell do not lead to a stabilization against fission in the deexcitation process of a compound nucleus in this region is of importance for the production of superheavy elements. Currently there exist plans to produce superheavy elements around the predicted spherical 184-neutron shell (e.g. Ref. [41]) by so called hot fusion, where a superheavy compound nucleus is formed which deexcites by evaporation of several (3–5) neutrons. It would appear that for nuclei in the vicinity of the predicted spherical 184-neutron shell the expected production cross sections, estimated on the basis of the intrinsic level densities, will be reduced by several orders of magnitude, depending on the length of the evaporation chain, if collective excitations are included. It is interesting to note, that

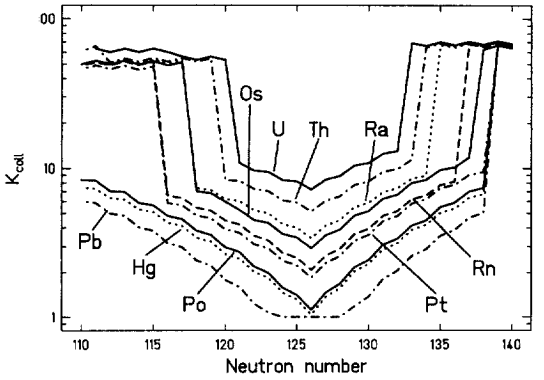

Fig. 8. The collective enhancement for even-Z isotopes from osmium to uranium calculated at an excitation energy of 10 MeV. The values belonging to one element are connected by lines.

the lack of shell stabilization against fission for actinides around $N = 126$ and its implication for the production of superheavy elements was already inferred from the analysis of fusion-evaporation data [42]. In conclusion, we emphasize again, that the production cross sections of spherical superheavy elements cannot be predicted correctly with an intrinsic level density including shell corrections without considering the collective (rotational and vibrational) enhancement.

5.3. *New results on the collective enhancement*

The collective enhancement as applied in the present work is shown in Fig. 8. At $|\beta_2| = 0.15$ there is a sharp transition from the rotational enhancement for deformed nuclei which amounts to $K_{rot} \approx 70$ to the vibrational enhancement for spherical nuclei with $K_{vib} \approx 1-10$. With this approach the production cross sections for all projectile fragments measured could be fairly well reproduced. The stabilization against fission for the neutron-deficient nuclei around $N = 126$ by the ground-state shell effects is compensated by the combined influence of the rotational enhancement of the level density at the saddle point and the vibrational enhancement in the spherical ground state.

The agreement of the full calculation including collective enhancement with the measured data in the interesting region around $N = 126$ for thorium, actinium, and radium shown in Figs. 3 and 5 is much better than for the calculation with the intrinsic level density including shell effects, but the isotopical dependence is not as smooth as that of the simple calculation disregarding any shell effects. This may be due to the sharp transition from rotational to vibrational enhancement used in our calculation without taking into account any transitional behaviour.

In order to describe our experimental data we were obliged to introduce a damping of the collective enhancement with excitation energy which is essentially *independent* of deformation. The damping is the same at the ground state and at the saddle point – a result which is in contradiction to the theoretical expectations of Refs. [1,2]. The question remains how well determined the values of $E_{cr} = 40$ MeV and $d_{cr} = 10$ MeV

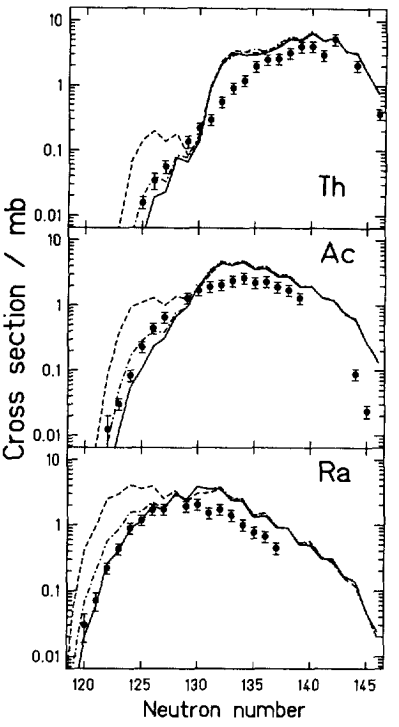

Fig. 9. Production cross sections of thorium, actinium, and radium fragments from 950 A MeV ^{238}U beam in a copper target are shown as data points. The lines show calculations including collective (rotational and vibrational) enhancement with different damping parameters E_{cr}, d_{cr}. The full lines are calculated with a very weak damping (E_{cr} = 80 MeV and d_{cr} = 10 MeV), while the dashed lines are calculated with a comparably strong damping (E_{cr} = 20 MeV and d_{cr} = 5 MeV). The dashed-dotted lines are the same as in Fig. 5 (E_{cr} = 40 MeV, d_{cr} = 10 MeV.)

suggested above are, and how these damping parameters relate to the washing out of the shell effects.

In Fig. 9 we compare the experimental cross sections of thorium, actinium, and radium isotopes with calculations involving different damping parameters. A damping of E_{cr} = 20 MeV and d_{cr} = 5 MeV which is stronger than the damping of the shell corrections leads to an incomplete cancellation of the shell stabilization and the collective enhancement. At an excitation energy of 20 MeV the collective enhancement already begins to vanish while a significant part of the shell stabilization is still in effect. Thus, the predicted cross sections are too high around the shell. When the damping is made weaker (E_{cr} = 80 MeV and d_{cr} = 10 MeV) than the damping used for the shell corrections, the predicted yields fall below the thorium and the actinium data. This discrepancy is much smaller compared to the case with E_{cr} = 20 MeV and d_{cr} = 5 MeV. A general good agreement with the data can be reached with E_{cr} = 40 MeV and d_{cr} = 10 MeV. In this case, the damping is comparable to the damping of the shell effects and leads to a quite complete cancellation of the shell stabilization by the collective enhancement.

5.4. Comparison to light-particle induced reactions

The analysis performed above revealed that the fragmentation cross sections are very sensitive to the specific properties of the nuclear level density. On this basis, new insight into the collective character of excited nuclei could be obtained. In the following, we would like to check these new results by comparing our model calculations with some of the available cross sections on ^{3,4}He- and proton-induced fission with targets around lead and below [17,18,36,43,20]. In these experiments, spherical nuclei with large shell effects (around 10 MeV) as well as strongly deformed nuclei have been investigated. In contrast to the nuclei near $N = 126$ produced by fragmentation of ^{238}U, these nuclei show rather low fission probabilities due to their large liquid-drop fission barriers, see Fig. 2. In order to show two typical examples, the fission probabilities of ^{210}Po and ^{188}Os from Ref. [18] are compared with our model including all structural and collective effects without adjusting any parameter, see Fig. 10. In the calculations, multiple-chance fission was taken into account to correctly describe the high-energy behaviour ($E^* \gtrsim 100$ MeV) of the fission probabilities. Obviously, it is possible to obtain a fair description of these data, too.

Another calculation shown in Fig. 10 uses a backshifted Fermi-gas level density. In this version, the level density is calculated from the Fermi-gas model with a fictitious basis corresponding to the liquid-drop ground state. The spirit of this calculation agrees with the calculation presented in Fig. 3 (dashed lines) which disregards any shell effects. It also corresponds to the recent description proposed by Moretto et al. [20], however with slightly different parameters. It may be stated that this option which disregards both the shell effects and the collective nuclear properties can describe the data nearly as well as the full calculation. The remaining deviations from the data are similar in magnitude as those between the different calculations.

As was shown in Ref. [20], a series of similar data can be reproduced much better when the parameters of the model are adapted to the data. The description found in that work was obtained by a three-parameter fit using the asymptotic level-density parameter ratio $\tilde{a}_f/\tilde{a}_n$, ($\tilde{a}_n = A/8$ MeV^{-1}), an effective fission barrier B_f^*, and the ground-state shell effect Δ_{shell} of the daughter nucleus after neutron evaporation as fitting variables. On the expense of fitting these parameters for every compound nucleus separately, a very good agreement with the experimental fission excitation functions could be obtained. A comparably good description of similar data was obtained in Ref. [19,16] including collective excitations, where a slightly different set of parameters was fitted to the data.

In contrast, it was not our aim to adjust any model parameters specifically to these data but to check whether the projectile fragmentation and the light-particle induced reactions can be described with the same set of parameters. It may be concluded that the fragmentation cross sections and the fusion-fission data can satisfactorily be described using the same assumptions for the statistical deexcitation phase. It seems that the deduced properties of the nuclear level density for spherical and deformed nuclei are fairly well represented by the description proposed in the present work.

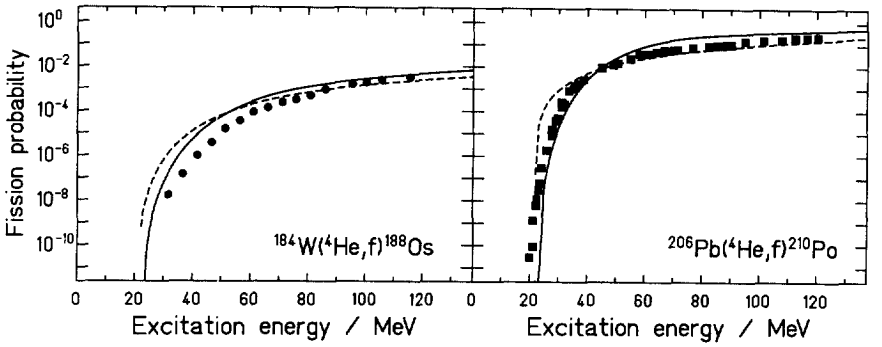

Fig. 10. Measured fission probabilities of ^{210}Po and ^{188}Os from Ref. [18] (data points) in comparison with two model calculations. Full lines: Full calculation with shell effects and collective nuclear properties included as proposed in this work. Dashed lines: Calculation with a backshifted Fermi-gas model (see text).

6. Conclusion

The analysis of the fragmentation cross sections performed in the present work revealed new information on the level density of spherical, transitional, and deformed nuclei. Characteristic differences of collective excitations in spherical and deformed configurations which are well established at energies a few MeV above the yrast line, from data of nuclear spectroscopy, were found to still persist up to about 40 MeV. Evidence for the loss of collectivity of nuclear excitations as a function of nuclear temperature has been found. The damping of the collective enhancement in the nuclear level density was found to be *independent* of nuclear deformation. The damping parameters deduced here correspond to the values suggested for the damping of the rotational enhancement in the ground-state deformation of deformed heavy nuclei [1,2]. With these parameters, the damping of the collective enhancement is comparable to the washing out of the ground-state shell effect. Moreover, an estimation for the magnitude and the energy dependence of the vibrational enhancement in spherical and transitional nuclei has been deduced. It was shown that the influence of shell stabilization and collective enhancement in the level density on the fissility of spherical nuclei cancel each other. As a practical consequence of the present analysis, the expected stabilizing influence of a strong spherical shell effect on the fission competition in the statistical deexcitation process was not found. Instead, the nucleus behaves very similar to a fictitious macroscopic nucleus without any shell effect in the binding energies and the level densities. This result has very important consequences for the expectations on the production cross sections of spherical superheavy nuclei near the 184-neutron shell. Estimations based on the intrinsic level density without inclusion of the collective enhancement overestimate the production cross sections drastically.

Acknowledgements

This work has been supported by the GSI Hochschulprogramm and by the Bundesministerium für Bildung, Wissenschaft, Forschung und Technologie under contract number BMBF 06 DA 473. The responsibility for the contents rests with the authors.

Appendix A

The Fermi-gas state density used in the abrasion–ablation model with shell and pairing corrections is described partially in Refs. [31,13]. Therefore, we want to give a short comprehensive overview.

The state density is expressed by

$$\rho = \frac{\sqrt{\pi}\exp(S)}{12\tilde{a}^{1/4}E^{5/4}},$$

with the entropy S

$$S = 2\sqrt{\tilde{a}(E + \delta U k(E) + \delta P h(E))},$$

and the asymptotic level-density parameter $\tilde{a}$ as given in Ref. [36]

$$\tilde{a} = 0.073A\ \mathrm{MeV}^{-1} + 0.095B_s A^{2/3}\ \mathrm{MeV}^{-1},$$

where B_s is the dimensionless surface area of a deformed nucleus. For saddle-point shapes, B_s is a function of the fissility parameter [44], while for a spherical ground-state $B_s = 1$. δU is the shell correction as calculated in the finite-range liquid-drop model [38]. $k(E) = 1 - \exp(-\gamma E)$ with $1/\gamma = 0.4A^{4/3}/\tilde{a}$ describes the damping of the shell effects with excitation energy. The function $k(E)$ has been adapted to give close agreement with microscopic calculations of the level density of heavy nuclei [11,13].

$$\delta P = -\tfrac{1}{4}\Delta^2 g + 2\Delta$$

is the effective pairing energy shift with an average pairing gap $\Delta = 12/\sqrt{A}$ MeV, and $g = \tilde{a}6/\pi^2$ is the single-particle level density at the Fermi energy.

$$h(E) = \begin{cases} 1 - \left(1 - \dfrac{E}{E_{\mathrm{crit}}}\right)^2 & \text{for } E < E_{\mathrm{crit}}, \\ 1 & \text{for } E \geqslant E_{\mathrm{crit}}, \end{cases}$$

$h(E)$ describes the washing out of the pairing correlations with the critical energy $E_{\mathrm{crit}} = 10$ MeV. The effective energy E is shifted with respect to the excitation energy E^* to accommodate for the different condensation energies of even–even, odd mass, and odd–odd nuclei.

$$\begin{aligned} E &= E^* && \text{odd–odd}, \\ E &= E^* - \Delta && \text{odd mass}, \\ E &= E^* - 2\Delta && \text{even–even}. \end{aligned}$$

References

[1] S. Bjørnholm, A. Bohr and B.R. Mottelson, Proc. Int. Conf. on the Physics and Chemistry of Fission, Rochester 1973 (IAEA Vienna 1974) Vol. 1, p. 367.
[2] G. Hansen and A.S. Jensen, Nucl. Phys. A 406 (1983) 236.
[3] A. Bohr, Mat. Fys. Medd. Dan. Vid. Selsk. 26 (1952) No. 14.

[4] A. Bohr, B.R. Mottelson, Mat. Fys. Medd. Dan. Vid. Selsk. 27 (1953) No. 16.
[5] A. Gilbert and A.G.W. Cameron, Can. J. Phys. 43 (1965) 1446.
[6] H. Baba, Nucl. Phys. A 159 (1970) 625.
[7] A.V. Ignatyuk, K.K. Istekov and G.N. Smirenkin, Yad. Fiz. 29 (1979) 875 (Sov. J. Nucl. Phys. 29 (1979) 450).
[8] V.S. Ramamurthy, S.S. Kapoor and S.K. Kataria, Phys. Rev. Lett. 25 (1970) 386.
[9] L.G. Moretto, Nucl. Phys. A 182 (1972) 641.
[10] A. Bohr and B.R. Mottelson, Nuclear Structure Vol. II (Benjamin, New York, 1975).
[11] A.V. Ignatyuk, G.N. Smirenkin and A.S. Tishin, Yad. Fiz. 21 (1975) 485 (Sov. J. Nucl. Phys. 21 (1975) 255).
[12] A.S. Jensen, J. Sandberg, Physica Scripta 17 (1978) 107.
[13] K.-H. Schmidt, H. Delagrange, J.P. Dufour, N. Cârjan and A. Fleury, Z. Phys. A 308 (1982) 215.
[14] A.V. Ignatyuk, K.K. Istekov and G.N. Smirenkin, Yad. Fiz. 30 (1979) 1205 (Sov. J. Nucl. Phys. 30 (1979) 626).
[15] A. Gavron, H.C. Britt, E. Konecny, J. Weber and J.B. Wilhelmy, Phys. Rev. C 13 (1976) 2374.
[16] A.S. Iljinov, M.V. Mebel, N. Bianchi, E. De Sanctis, C. Guaraldo, V. Lucherini, V. Muccifora, E. Polli, A.R. Reolon and P. Rossi, Nucl. Phys. A 543 (1992) 517.
[17] A. Khodai-Joopary, Ph.D. thesis, University of California, Lawrence Radiation Laboratory, UCRL-16489 (1966).
[18] L.G. Moretto, S.G. Thompson, J. Routti and R.C. Gatti, Phys. Lett. B 38 (1972) 471.
[19] A.V. Ignatyuk, G.N. Smirenkin, M.G. Itkis, S.I. Mul'gin and V.N. Okolovich, Fiz. Elem. Chastits At. Yadra 16 (1985) 709 (Sov. J. Part. Nucl. 16 (1985) 307).
[20] L.G. Moretto, K.X. Jing, R. Gatti, G.J. Wozniak and R.P. Schmitt, Phys. Rev. Lett. 75 (1995) 4186.
[21] J.R. Huizenga and L.G. Moretto, Ann. Rev. Nucl. Sci. 22 (1972) 427.
[22] D. Vermeulen, H.-G. Clerc, C.C. Sahm, K.-H. Schmidt, J.G. Keller, G. Münzenberg and W. Reisdorf, Z. Phys. A 318 (1984) 157.
[23] C.-C. Sahm, H.-G. Clerc, K.-H. Schmidt, W. Reisdorf, P. Armbruster, F.P. Hessberger, J.G. Keller, G. Münzenberg and D. Vermeulen, Nucl. Phys. A 441 (1985) 316.
[24] A.V. Ignatyuk, K.K. Istekov and G.N. Smirenkin, Yad. Fiz. 37 (1983) 831 (Sov. J. Nucl. Phys. 37 (1983) 495).
[25] K.-H. Schmidt, J.G. Keller and D. Vermeulen, Z. Phys A 315 (1984) 159.
[26] A.R. Junghans et al., to be published.
[27] M. de Jong, A.V. Ignatyuk and K.-H. Schmidt, Nucl. Phys. A 613 (1997) 435.
[28] K.-H. Schmidt and W. Morawek, Rep. Prog. Phys. 54 (1991) 949.
[29] H.-G. Clerc, M. de Jong, T. Brohm, M. Dornik, A. Grewe, E. Hanelt, A. Heinz, A. Junghans, C. Röhl, S. Steinhäuser, B. Voss, C. Ziegler, K.-H. Schmidt, S. Czajkowski, H. Geissel, H. Irnich, A. Magel, G. Münzenberg, F. Nickel, A. Piechaczek, C. Scheidenberger, W. Schwab, K. Sümmerer, W. Trinder, M. Pfützner, B. Blank, A.V. Ignatyuk and G.A. Kudyaev, Nucl. Phys. A 590 (1995) 785.
[30] M. de Jong, K.-H. Schmidt, B. Blank, C. Böstiegel, T. Brohm, H.-G. Clerc, S. Czajkowski, M. Dornik, H. Geissel, A. Grewe, E. Hanelt, A. Heinz, H. Irnich, A. Junghans, A. Magel, G. Münzenberg, F. Nickel, M. Pfützner, A. Piechaczek, C. Scheidenberger, W. Schwab, S. Steinhäuser, K. Sümmerer, W. Trinder, B. Voss and C. Ziegler, Nucl. Phys. A 628 (1998) 479.
[31] J.-J. Gaimard and K.-H. Schmidt, Nucl. Phys. A 531 (1991) 709.
[32] K.-H. Schmidt, T. Brohm, H.-G. Clerc, M. Dornik, M. Fauerbach, H. Geissel, A. Grewe, E. Hanelt, A. Junghans, A. Magel, W. Morawek, G. Münzenberg, F. Nickel, M. Pfützner, C. Scheidenberger, K. Sümmerer, D. Vieira, B. Voss and C. Ziegler, Phys. Lett. B 300 (1993) 313.
[33] X. Campi, H. Krivine and E. Plagnol, Phys. Rev. C 50 (1994) R2680.
[34] K.-H. Schmidt, K. Sümmerer, H. Geissel, G. Münzenberg, F. Nickel, M. Pfützner, M. Weber, B. Voss, T. Brohm, H.-G. Clerc, M. Fauerbach, J.-J. Gaimard, A. Grewe, E. Hanelt, M. Steiner, J. Weckenmann, C. Ziegler and A. Magel, Nucl. Phys. A 542 (1992) 699.
[35] A.V. Ignatyuk, G.A. Kudyaev, A. Junghans, M. de Jong, H.-G. Clerc and K.-H. Schmidt, Nucl. Phys. A 593 (1995) 519.
[36] A.V. Ignatyuk, M.G. Itkis, V.N. Okolovich, G.N. Smirekin and A.S. Tishin, Yad. Fiz. 21 (1975) 1185 (Sov. J. Nucl. Phys. 21 (1975) 612).
[37] A.J. Sierk, Phys. Rev. C 33 (1986) 2039.
[38] P. Möller, J.R. Nix, W.D. Myers and W.J. Swiatecki, At. Data Nucl. Data Tables 59 (1995) 185.

[39] S. Cohen and W.J. Swiatecki, Ann. Phys. 22 (1963) 406.
[40] S. Raman, C.W. Nestor, Jr., S. Kahane and K.H. Bhatt, At. Data and Nucl. Data Tables 42 (1989) 1.
[41] S.Ćwiok and A. Sobiczewski, Z. Phys. A 342 (1992) 203.
[42] K.-H. Schmidt, W. Faust, G. Münzenberg, W. Reisdorf, H.-G. Clerc, D. Vermeulen, W. Lang, Proc. Int. Conf. on the Physics and Chemistry of Fission, Jülich 1979 (IAEA Vienna 1980) Vol. 1, p. 409.
[43] A.V. Ignatyuk, M.G. Itkis, I.A. Kamenev, S.I. Mul'gin, V.N. Okolovich and G.N. Smirenkin, Yad. Fiz. 40 (1984) 625 (Sov. J. Nucl. Phys. 40 (1984) 400).
[44] W.D. Myers and W.J. Swiatecki, Ann. Phys. 84 (1974) 186.